Materials Science and Engineering: A (2012). 534, 624-631.
DOI: http://dx.doi.org/10.1016/j.msea.2011.12.019

Hot deformation behaviour and flow stress prediction of 7075 aluminium alloy powder compacts during compression at elevated temperatures

M.A. Jabbari Taleghani [a,*], E.M. Ruiz Navas [b], M. Salehi [c], J.M. Torralba [a]

[a] Institute IMDEA Materials, Universidad Carlos III De Madrid, Av. Del Mar Mediterráneo 22, 28918 Leganés, Spain
[b] Department of Materials Science and Engineering, Universidad Carlos III De Madrid, Av. Universidad 30, 28911 Leganés, Spain
[c] Department of Materials Engineering, Isfahan University of Technology, Isfahan 84156-83111, Iran

* Corresponding author. Tel.: +34 91 549 34 22; fax: +34 91 550 30 47. *E-mail addresses:* mohammad.jabbari@imdea.org, mo.jabbari@yahoo.com

Abstract: In the present study, the hot deformation behaviour of 7075 aluminium alloy powder compacts was studied by performing hot compression tests on a Gleeble 3800 machine. The main objectives were to evaluate the effect of the relative green density on the hot deformation behaviour and to model and predict the hot deformation flow stress of powder compacts using constitutive equations. For this pur-pose, powder compacts with relative green densities ranging from 83 to 95%, which were prepared by uniaxial cold pressing a commercial pre-mixed powder, were hot compressed at temperatures ranging from 350 °C t o 4 5 0 °C and at true strain rates ranging from 0.01 s^{-1} to 10 s^{-1}. The true stress–true strain curves of the powder compacts exhibited a peak stress at a critical strain after which the flow stress remained nearly constant. As the deformation temperature increased or the strain rate and green density decreased, a decrease in the peak stress level was observed. The relationship between deformation tem-perature, strain rate, and the peak flow stress of powder compacts was described by the Zener–Hollomon parameter in an exponential equation containing relative green density compensated material constants and the deformation activation energy. The peak flow stresses calculated from the proposed formula were in good agreement with the experimental results, which confirms the applicability of the employed method for the prediction of the hot deformation flow stress of porous materials with different relative green densities.

Keywords: Al–Zn–Mg–Cu aluminium alloy, Premixed powder, Hot compression, Flow curve, Constitutive equation, Flow stress prediction.

1. Introduction

7xxx series aluminium alloys based on ternary Al–Zn–Mg or quaternary Al–Zn–Mg–Cu alloying systems have an interesting combination of such properties as high strength, high fracture toughness, low density, good workability, favourable weldability, and remarkable resistance to stress corrosion cracking. Therefore, these alloys have long been regarded as some of the best candidates for demanding structural applications in the aerospace and automotive industries. Among commercial aluminium alloys, 7xxx series alloys show the highest strength [1–6].

In aluminium powder metallurgy (PM), the superior properties of aluminium are combined with the ability of PM to produce high performance net- or near-net-shaped parts, which can reduce or eliminate the capital and operational costs associated with intricate machining operations [7,8]. In addition, atomised powders of aluminium and its alloys have a fine and homogeneous microstructure, which leads to after-consolidation mechanical properties that cannot be attained through the conventional processing of cast and wrought alloys with similar chemical compositions [8]. Powder extrusion (PE) and powder forging (PF) are the most promising PM processing methods which have been developed for the production of fully dense, high-performance materials from powders [9,10].

A good understanding of the hot deformation behaviour of a material is extremely important in hot deformation processes such as extrusion and forging [11–13]. Processing parameters, such as the deformation temperature and strain rate, and material factors, such as chemical composition and microstructure of the starting material, are the main factors affecting the hot deformation flow stress. Thus, several studies have been performed to investigate the effect of processing parameters on the hot deformation behaviour of aluminium and its alloys [3,6,14–16]. Furthermore, the flow stress behaviour of these materials has been modelled, and constitutive equations that consider the effects of the deformation temperature and strain rate have been proposed to predict the hot deformation flow stress [13,17,18].

The hot deformation behaviour of bulk aluminium alloys has been the subject of many studies [3,6,7,14–16,19–21]. Nevertheless, the deformation behaviour of porous materials is different

Table 1
The effect of the cold pressing pressure on the relative green density (RGD) of powder compacts.

Pressing pressure (MPa)	RGD (%)
200	83
300	88.5
500	94
700	95

from that of bulk materials. Pores present in the microstructure act as stress concentration points, limiting the amount of deformation to fracture [22]. Moreover, the volume of voids is reduced during deformation, which results in an increase in density and densification. In addition to strain hardening, densification during deformation can enhance the flow stress of the material, which is known as densification hardening [23]. In the case of powder-based porous materials, such as powder compacts, due to friction between particles, redundant work is required to weld powder particles together, break welds between particles, and re-weld them together [10]. Thus, information on the deformation behaviour of bulk aluminium alloys is not usable for the deformation of porous alloys with similar chemical compositions.

Studies on the hot deformation behaviour of porous aluminium alloys are relatively scarce [22–25]. Due to the lack of knowledge in the field [23] and the importance of constitutive information for the modelling of powder processing routes such as PE and PF [11,12], the effects of the relative green density, deformation temperature, and strain rate on the hot deformation behaviour and flow stress of powder compacts cold pressed from a commercial Al–Zn–Mg–Cu premix were evaluated in the present study. In addition, a constitutive equation that is capable of predicting the peak flow stress of powder compacts and considers the relative green density, deformation temperature, and strain rate was proposed.

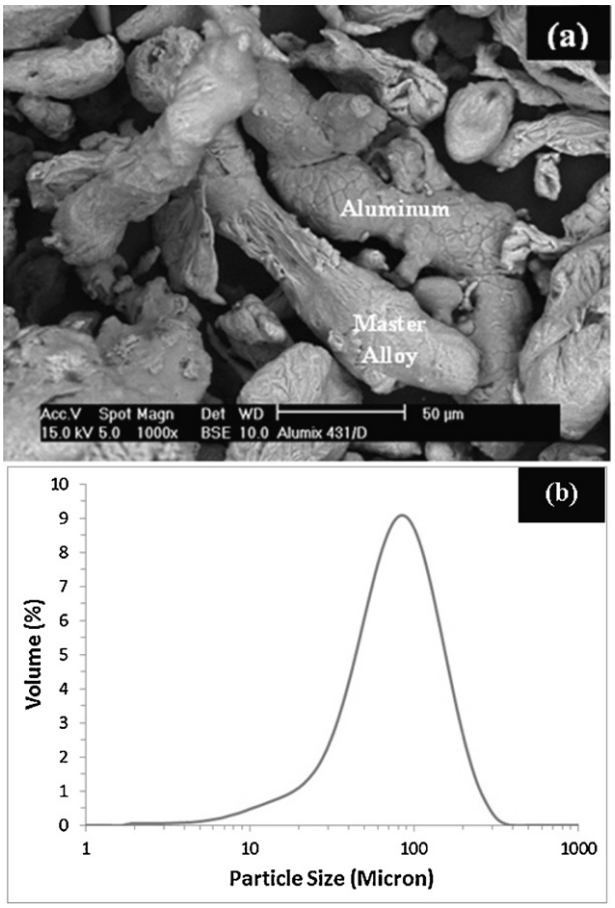

Fig. 1. Morphology (a) and particle size distribution (b) of the as-received powder.

2. Experimental procedure

A commercially available premixed Al–Zn–Mg–Cu powder, Alumix 431D (Ecka Granules, Germany), with a chemical composition similar to AA 7075 alloy (5.6–6.4 wt% Zn, 2.4–3 wt% Mg, 1.5–2 wt% Cu, 0.1–0.3 wt% Sn, and the balance Al) was used in the current investigation. The main component of the premix was atomised aluminium powder, which was mixed with a master alloy powder containing all of the alloying elements. Because the premix was a ready-to-press blend, it contained approximately 1.5% lubricant to facilitate the pressing step. Fig. 1 shows the morphology and particle size distribution of the premix. The grain structures of aluminium particles are detectable on their surfaces (Fig. 1(a)). The particles of the premix possessed an irregular and elongated morphology, which is typical of atomised aluminium-based powders. The average particle size of the mixture was 80 μm.

The premix was uniaxially cold pressed into cylindrical billets with a diameter of 10 mm and a length of 15 mm. To produce powder compacts with dissimilar green densities, different compaction pressures were used. The pressures applied during pressing and the corresponding relative green densities are listed in Table 1. The green densities of compacts were measured by both Archimedes' method following MPIF 42 standard test method and direct calculation of volume and dividing it by weight.

Different cold pressing pressures produce different green densities and levels of strain hardening, which both affect the deformation behaviour of powder compacts. Because the aim of the present study was to investigate the effect of the relative green density on the deformation behaviour, other factors that can affect the deformation behaviour of powder compacts were eliminated. Therefore, to minimise the effect of strain hardening due to cold compaction on the hot deformation behaviour, the powder compacts were subjected to a stress relief heat treatment (the compacts were heated to 400 °C at a rate of 5 °C s^{-1}, maintained at 400 °C for 20 min, and furnace-cooled to room temperature) in a high-purity nitrogen atmosphere.

A graphite foil with a thickness of 0.05 mm was placed between the ends of the powder compacts and the anvils to minimise friction during the compression test. Prior to the compression tests, the samples were resistance-heated under vacuum to the required temperature at a heating rate of 5 °C s^{-1} and were maintained at the test temperature for 1 min to minimise thermal gradients along the sample. Single-hit compression tests were carried out using a servo-controlled Gleeble-3800 system at strain rates of 0.01 s^{-1}, 0.1 s^{-1}, 1 s^{-1}, and 10 s^{-1} and deformation temperatures of 350 °C, 400 °C, and 450 °C. After the compression tests, the samples were cooled to room temperature at a cooling rate of approximately 10 °C s^{-1}.

3. Results and discussion

3.1. Flow stress curves

A series of typical true stress–true strain curves obtained during the hot compression of Alumix 431D powder compacts with different relative green densities at various temperatures and strain rates are shown in Figs. 2–4.

For most of samples, the true stress–true strain curves exhibited a peak stress at a critical strain after which the flow stress remained nearly constant. However, for some of samples, after reaching the peak the flow stresses decreased continuously, showing a dynamic

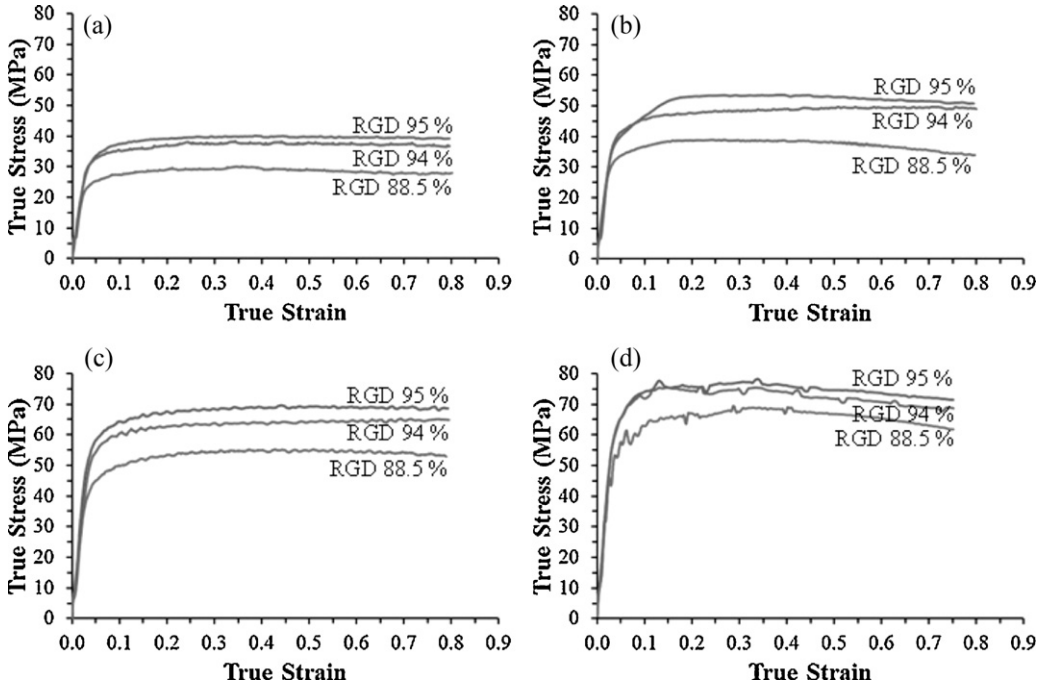

Fig. 2. True stress-true strain curves of Alumix 431 D powder compacts hot compressed at 350 °C and different strain rates: (a) $\dot{\varepsilon} = 0.01\ s^{-1}$, (b) $\dot{\varepsilon} = 0.1\ s^{-1}$, (c) $\dot{\varepsilon} = 1\ s^{-1}$, and (d) $\dot{\varepsilon} = 10\ s^{-1}$.

flow softening. As the deformation temperature increased or the strain rate and green density decreased, a decrease in the peak stress level was observed.

During the deformation of porous materials at high temperatures, hardening mechanisms, such as strain and densification hardening, and softening mechanisms, such as dynamic recovery and recrystallisation, can occur simultaneously. At the beginning of deformation, the dislocation density increases rapidly, which leads to a sharp increase in the flow stress [6]. As deformation continues, the activation of dynamic softening mechanisms can partially or completely neutralise the effect of hardening mechanisms [3,7,26]. As a result, the slope of the flow stress flattens and may even become zero. In some materials, dynamic softening can cause the flow stress to decrease after reaching a maximum value [14,15].

In the present study, the observed decrease in the flow stress, which occurred during the hot compression test at a strain rate of $10\ s^{-1}$, can be associated with the cracking and heating of samples. The formation of cracks reduces the resistance of the material to deformation, which decreases the flow stress. High strain rate

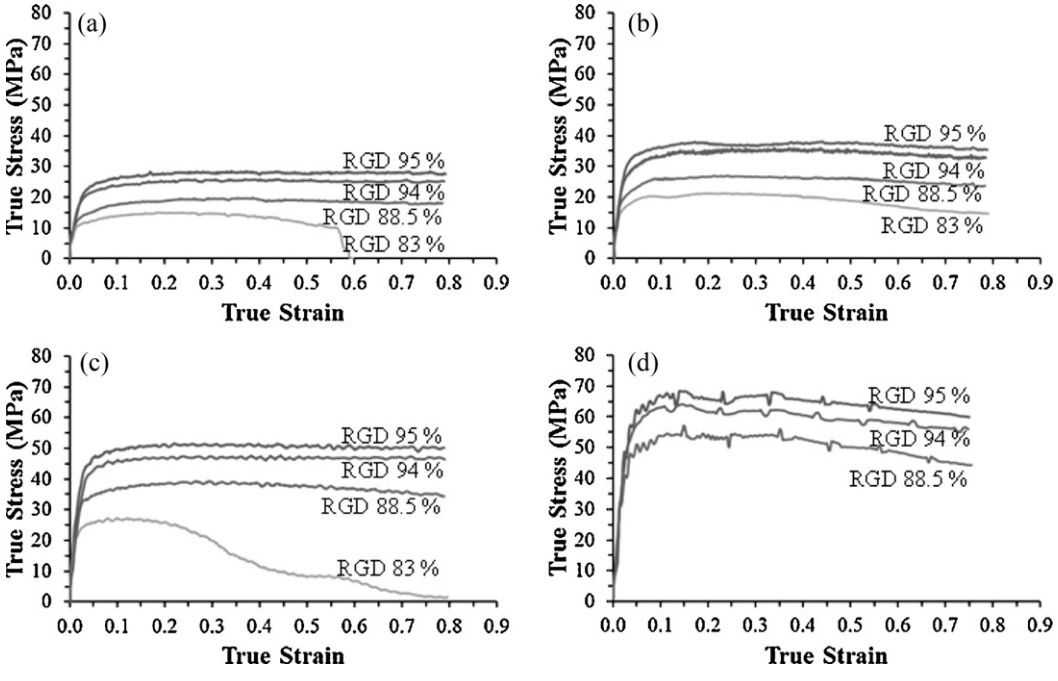

Fig. 3. True stress-true strain curves of Alumix 431 D powder compacts hot compressed at 400 °C and different strain rates: (a) $\dot{\varepsilon} = 0.01\ s^{-1}$, (b) $\dot{\varepsilon} = 0.1\ s^{-1}$, (c) $\dot{\varepsilon} = 1\ s^{-1}$, and (d) $\dot{\varepsilon} = 10\ s^{-1}$.

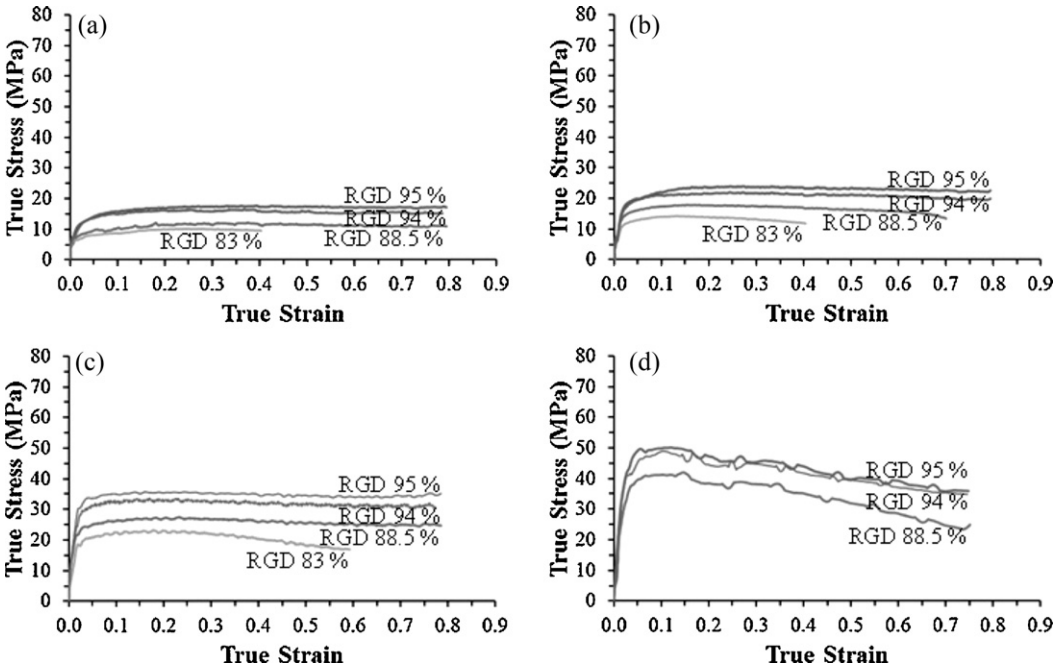

Fig. 4. True stress-true strain curves of Alumix 431 D powder compacts hot compressed at 450 °C and different strain rates: (a) $\dot{\varepsilon} = 0.01\ s^{-1}$, (b) $\dot{\varepsilon} = 0.1\ s^{-1}$, (c) $\dot{\varepsilon} = 1\ s^{-1}$, and (d) $\dot{\varepsilon} = 10\ s^{-1}$.

deformation processes are essentially adiabatic. Thus, the temperature of the sample can rise during deformation, which decreases the flow stress of the material and leads to thermal softening [7,15,16,22,26]. Fig. 5 shows the specimen temperatures (T_m) measured during the compression tests of powder compacts with a relative green density of 94% at a temperature of 400 °C and strain rates of 0.01 and 10 s^{-1}. It can be seen that during the compression test at the strain rate of 0.01 s^{-1}, the specimen temperature was almost constant and equal to the pre-set temperature of 400 °C. However, at the strain rate of 10 s^{-1}, the temperature of the sample rose continuously during the compression test, suggesting a significant role for deformation heating in flow softening at this strain rate.

Due to the high degree of porosity (17%), compacts cold pressed at a pressure of 200 MPa were notably brittle. As a result, at high strains (strains greater than 0.3), these compacts were susceptible to cracking and breaking. Consequently, after the peak stress, a reduction in the flow stress was detected for most of these samples (Figs. 3 and 4(c)).

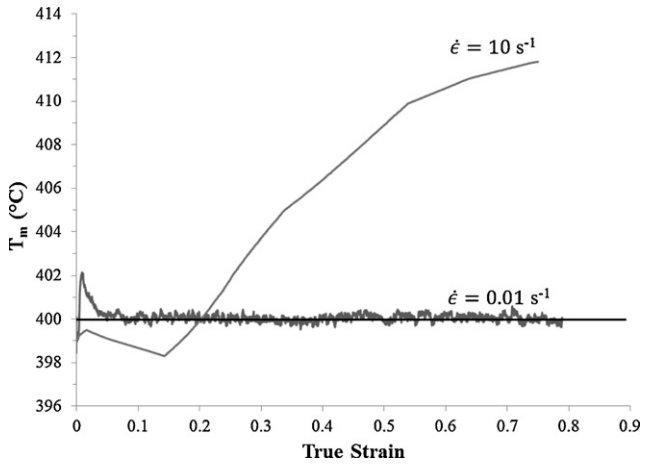

Fig. 5. Specimen temperatures (T_m) measured during the compression tests of powder compacts with a relative green density of 94% at a pre-set temperature of 400 °C and strain rates of 0.01and 10 s^{-1}.

3.2. Constitutive analysis

In the hot deformation of metallic materials, the relationship between the peak flow stress or steady-state flow stress of the material and deformation parameters, such as the deformation temperature and strain rate, can be expressed as [27]:

$$Z = \dot{\varepsilon} \exp\left(\frac{Q}{RT}\right) = F(\sigma) \tag{1}$$

$$\dot{\varepsilon} = Z \exp\left(-\frac{Q}{RT}\right) = F(\sigma)\exp\left(-\frac{Q}{RT}\right) \tag{2}$$

where Z (Zener–Hollomon parameter) is the temperature-corrected strain rate, $\dot{\varepsilon}$ is the strain rate (s^{-1}), Q is the activation energy of hot deformation (J/mol), R is the gas constant (8.31 J mol^{-1} K^{-1}), and T is the absolute temperature (K). $F(\sigma)$ is called the stress function and corresponds to one of the following equations depending on the deformation conditions:

$$F(\sigma) = A_1\sigma^m = Z \tag{3}$$

$$F(\sigma) = A_2\exp(\beta\sigma) = Z \tag{4}$$

$$F(\sigma) = A_3[\sinh(\alpha\sigma)]^n = Z \tag{5}$$

where A_1, A_2, A_3, m, β, and n are constants of the material. α is the stress multiplier and is a constant that brings $\alpha\sigma$ into the correct range, forming parallel and linear plots of (ln $\dot{\varepsilon}$) versus (ln sinh ($\alpha\sigma$)).

Eq. (3), i.e., the power law stress function, is commonly used for deformation processes that require low stress levels, such as creep, while Eq. (4), i.e., the exponential law stress function, is used for higher levels of stress and strain rates. Alternatively, the hyperbolic sine law stress function (Eq. (5)) can be used for a wide range of stress levels.

In all of the aforementioned equations, the flow stress is a function of the deformation temperature and strain rate (i.e., deformation parameters). However, the effect of strain on the flow stress

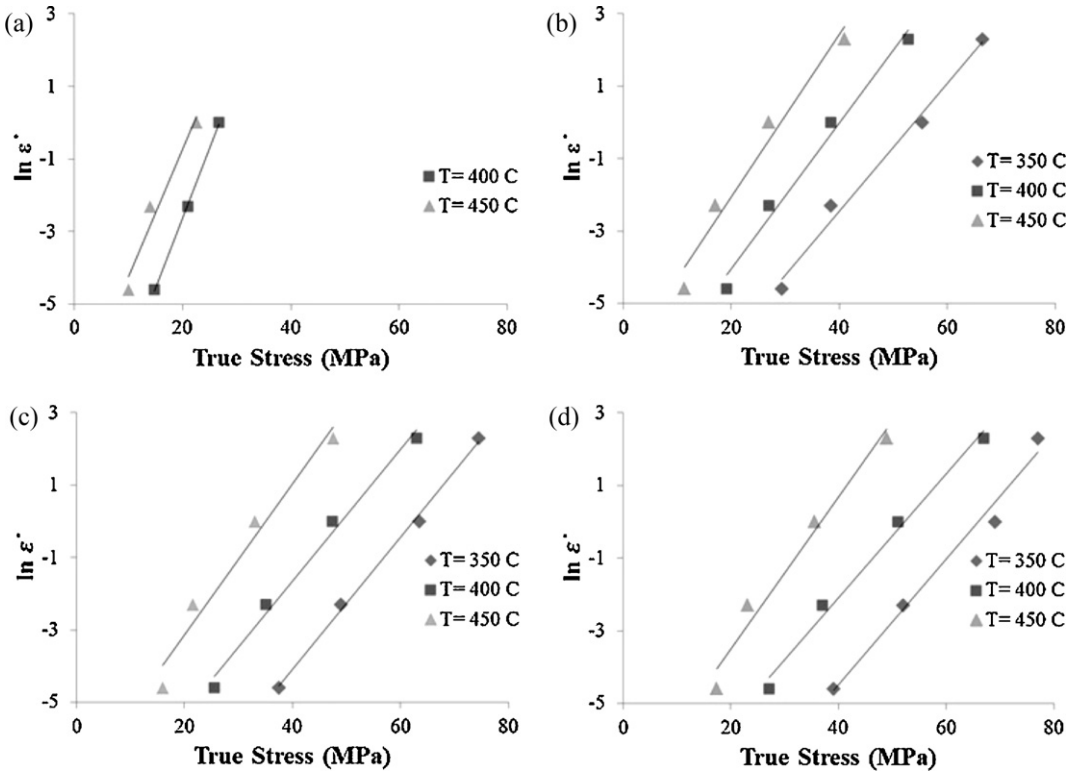

Fig. 6. Relationship between $\ln \dot{\varepsilon}$ and peak flow stress (true stress) for powder compacts with different relative green densities (RGD): RGD = 83% (a), RGD = 88.5% (b), RGD = 94% (c), and RGD = 95% (d).

is not considered in these equations. Therefore, characteristic flow stresses, such as the peak flow stress or steady-state flow stress, are commonly used in the equations. When strain hardening or flow softening is remarkable, the effect of strain on the flow stress should also be included.

In the present study, for most of the samples, the flow stress reached a peak and remained constant thereafter. Thus, the effect of strain on the flow stress was not considered; and the peak flow stress was used to model the flow stress behaviour of powder compacts.

As previously mentioned, the exponential law stress function (Eq. (4)) is suitable for high-stress level deformation processes, such as hot compression. By substituting $F(\sigma)$ from Eq. (4) into Eq. (1) and taking the natural logarithm, the following equations were derived:

$$A \exp(\beta\sigma) = \dot{\varepsilon} \exp\left(\frac{Q}{RT}\right) \tag{6}$$

$$\ln A + \beta\sigma = \ln \dot{\varepsilon} + \frac{Q}{RT} \tag{7}$$

$$\ln \dot{\varepsilon} = \beta\sigma + \ln A - \frac{Q}{RT} \tag{8}$$

$$\sigma = \frac{1}{\beta}\frac{Q}{RT} + \frac{1}{\beta}(\ln \dot{\varepsilon} - \ln A) \tag{9}$$

When T is constant, β is the slope of the plot of $\ln \dot{\varepsilon}$ versus σ (Eq. (8)). In contrast, when $\dot{\varepsilon}$ is constant, Q can be calculated from the slope of the plot of σ versus $(1/T)$ (Eq. (9)). The value of $\ln \dot{\varepsilon}$ as a function of the peak flow stress (true stress, σ) at a constant temperature for different powder compacts is shown in Fig. 6. The average slope of the lines obtained at a constant temperature for each powder compact was considered to be an estimate of the value of β for each powder compact. Subsequently, these values were used to calculate the deformation activation energy (Q) of each powder compact.

The value of peak flow stress (true stress, σ) as a function of $(1/T)$ at a constant strain rate for different powder compacts is shown in Fig. 7. The average slope of the lines obtained at a constant strain rate for each powder compact was used to calculate the value of Q for each powder compact. Based on Eq. (9), Q is equal to:

$$Q = R\beta\frac{d\sigma}{d(1/T)} \tag{10}$$

Table 2 presents the values of β and Q for each powder compact, which were obtained from Figs. 6 and 7.

The relative green density of the compact has a remarkable effect on the value of Q and β. Q, the hot deformation activation energy, is an indicator of the degree of difficulty of deformation. Namely, as the deformation activation energy increases, deformation becomes more difficult. As shown in the table, the value of Q decreased with a decrease in the relative green density. Thus, pores present in the structure of porous materials reduce the resistance to deformation. In contrast to Q, β was higher for powder compacts with lower relative green densities. The values obtained for the hot deformation activation energy were in good agreement with those previously reported for 7xxx series aluminium alloys [3,6,21,28,29]. Eq. (4) can be transformed as follows:

$$\ln Z = \ln A + \beta\sigma \tag{11}$$

The value of $\ln Z$ as a function of the peak flow stress (true stress, σ) for different compacts is presented in Fig. 8. As shown in the figure, a good linear relationship between $\ln Z$ and σ was observed for all of the samples. According to Eq. (11), $\ln A$ is the intercept of the

Table 2
The value of β and Q for powder compacts with different relative green densities.

Pressing pressure (MPa)	RGD (%)	β	Q (kJ/mol)
200	83	0.368	158
300	88.5	0.201	175
500	94	0.192	190
700	95	0.184	192

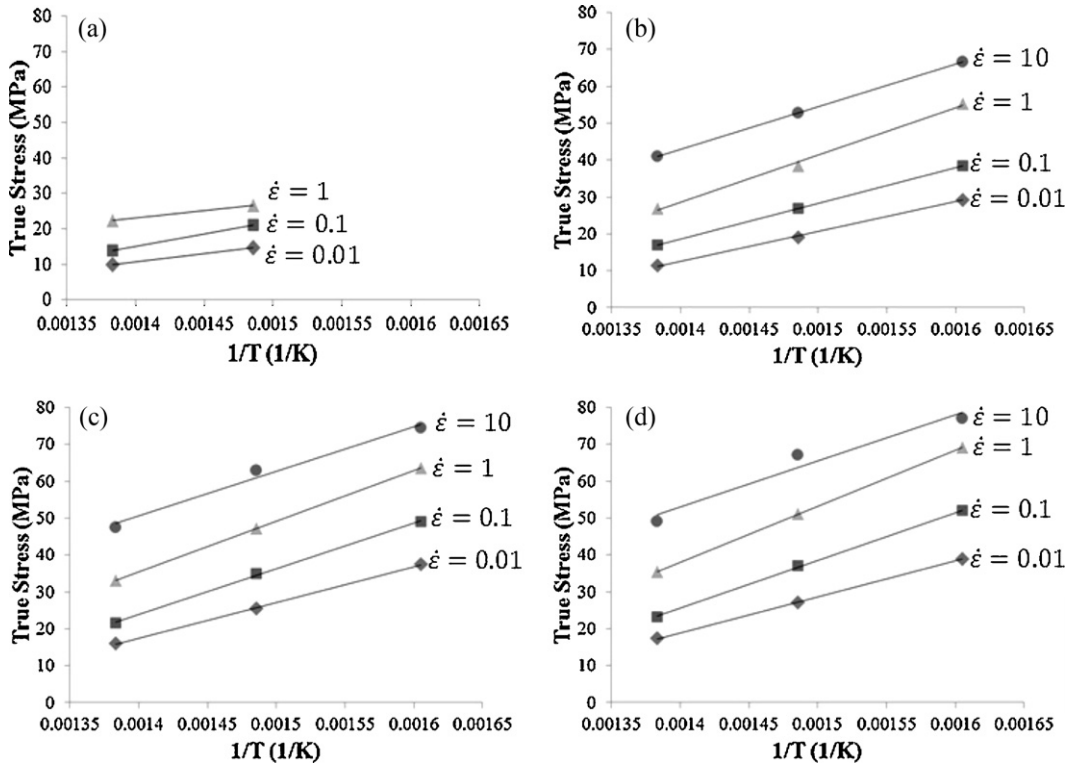

Fig. 7. Relationship between the peak flow stress (true stress) and (1/*T*) for powder compacts with different relative green densities (RGD): RGD = 83% (a), RGD = 88.5% (b), RGD = 94% (c), and RGD = 95% (d).

plot of ln *Z* versus σ; therefore, the value of *A* can be calculated for each powder compact. Moreover, the slope of the plot is equal to β, which was considered to be the β constant of each powder compact and used to model the peak flow stress of powder compacts with different relative green densities. The calculated values of β and *A* for each powder compact are shown in Table 3.

As shown in Table 3, as the relative green density decreased, the value of β increased. Because β is the slope of the plot of ln *Z* versus σ, when the value of β for a powder compact is high, significant changes in ln *Z*, i.e. deformation condition, slightly affect the peak flow stress of the powder compact (σ). In other words, compared to powder compacts with low values of β, the peak flow stress of a powder compact with a high β value is less dependent on deformation parameters, such as the deformation temperature and strain rate.

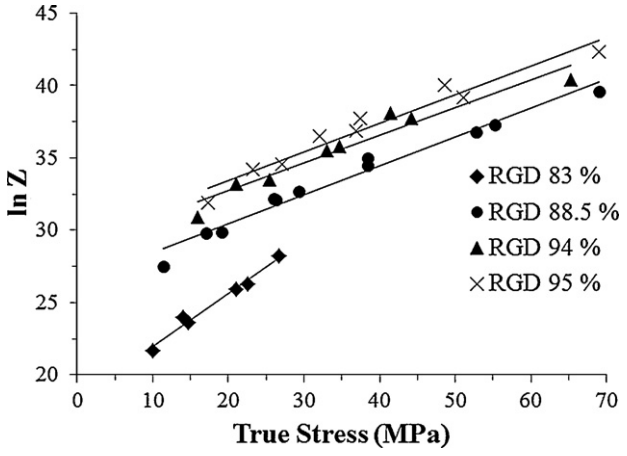

Fig. 8. Relationship between ln *Z* and the peak flow stress (true stress) of powder compacts with different relative green densities (RGD).

The relationships between β, ln *A*, and *Q*, and the relative green density of the powder compact are shown in Fig. 9 and can be fitted to a third-degree polynomial curve (solid lines), showing the evolution of β, ln *A*, and *Q* with the relative green density. Thus, the relationship between relative green density, strain rate, deformation temperature, and the flow stress of the powder compact can be expressed as follows (R^2 is the multiple correlation coefficient of each adjustment):

$$Z = \dot{\varepsilon} \exp\left(\frac{Q}{RT}\right) = A \exp(\beta\sigma) \tag{12}$$

$$\beta = -0.0003(RGD)^3 + 0.0842(RGD)^2 - 7.6957(RGD) + 234.62 \quad (R^2 = 1) \tag{13}$$

$$\ln A = 0.0035(RGD)^3 - 0.9901(RGD)^2 + 93.095(RGD) - 2898.8 \quad (R^2 = 1) \tag{14}$$

$$Q = -0.0066(RGD)^3 + 1.7111(RGD)^2 - 145.4(RGD) + 4194.5 \quad (R^2 = 1) \tag{15}$$

Table 3
The calculated values of β and *A* for powder compacts with different relative green densities.

Pressing pressure (MPa)	RGD (%)	β	ln *A*	*A*
200	83	0.368	18.3	9E+07
300	88.5	0.198	23.3	1E+10
500	94	0.190	24.9	6E+10
700	95	0.182	25.1	8E+10

Table 4
The predicated and experimental peak flow stresses (PFS) of powder compacts used for the development of the model.

Compression temperature (K)	Strain rate (1/s)	RGD = 83%			RGD = 88.5%			RGD = 94%			RGD = 95%		
		Exp. PFS	Calc. PFS	Error (%)	Exp. PFS	Calc. PFS	Error (%)	Exp. PFS	Calc. PFS	Error (%)	Exp. PFS	Calc. PFS	Error (%)
623	0.01	–	–	–	29.3	30.0	2.2	37.5	38.3	2.2	39.0	40.8	4.7
623	0.1	–	–	–	38.4	41.6	8.2	49.0	50.4	2.9	52.0	53.5	2.9
623	1	–	–	–	55.2	53.2	3.8	63.5	62.5	1.5	69.0	66.2	4.2
623	10	–	–	–	66.5	64.8	2.6	74.5	74.6	0.2	77.0	78.8	2.4
673	0.01	14.7	14.5	1.1	19.1	17.3	9.5	25.5	24.0	5.9	27.1	25.7	5.4
673	0.1	21	20.8	0.9	27.0	28.9	7.0	35.0	36.1	3.1	36.9	38.3	3.7
673	1	26.7	27.1	1.4	38.5	40.5	5.2	47.3	48.2	1.8	51.1	51.0	0.2
673	10	–	–	–	52.8	52.1	1.3	63.0	60.3	4.3	67.0	63.6	5.0
723	0.01	10	9.2	7.7	11.3	6.4	43.9	15.9	11.6	27.3	17.3	12.6	27.4
723	0.1	14	15.5	10.7	17.0	18.0	5.4	21.5	23.7	10.2	23.2	25.2	8.8
723	1	22.5	21.8	3.3	27.0	29.6	9.5	33.1	35.8	8.2	35.5	37.9	6.8
723	10	–	–	–	41.0	41.2	0.4	47.5	47.9	0.8	49.0	50.6	3.2

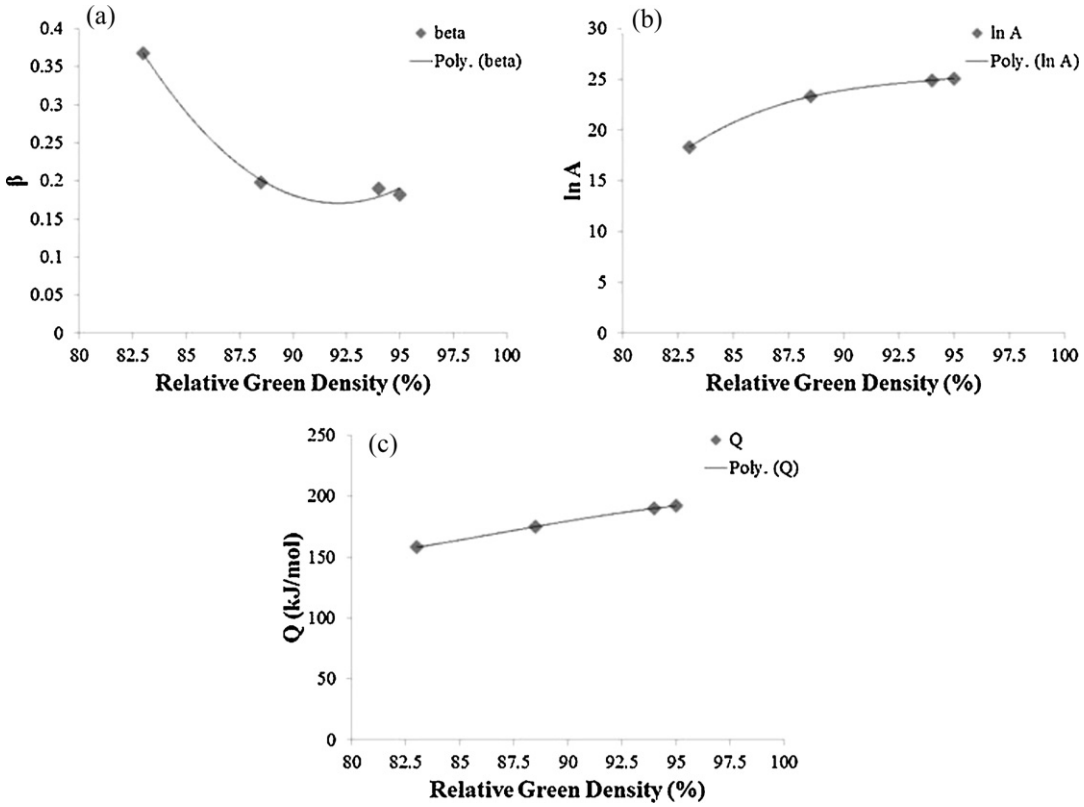

Fig. 9. Relationships between β (a), ln A (b), and Q (c), and the relative green density of the powder compact.

3.3. Flow stress prediction

In Table 4, the peak flow stresses calculated according to Eqs. (12)–(15) are compared to the experimental peak flow stresses of compacts used for the development of the model. As shown in the table, good agreement between the predicted and experimental values was observed, implying the good predictive capability of the developed model. The average error for compression temperatures of 350, 400, and 450 °C were 3.1, 3.7, and 11.6% respectively, suggesting that the predictive capability of the model is better for lower deformation temperatures. Furthermore, the average error for the compacts compressed at a temperature of 450 °C and strain rates of 0.01, 0.1, 1, and 10 s^{-1} were 26.6, 8.8, 7, and 1.5% respectively. It can be concluded that the predictive capability of the model is limited under the deformation condition of 450 °C and 0.01 s^{-1}.

Table 5 presents the calculated values of average error and root mean square error (RMSE) of the compacts. The maximum average error of the compacts was 8%. Considering the complexity of the deformation behaviour of porous materials, the observed degree of error for the prediction of flow stress is acceptable and confirms the applicability of the proposed equations for the prediction of the

Table 5
The calculated values of average error and RMSE of powder compacts used for the development of the model.

RGD (%)	Average of error (%)	RMSE (MPa)
83	4.2	0.8
88.5	8.2	2.3
94	5.7	2
95	6.2	2.4

Table 6
Predicated and experimental peak flow stresses (PFS) of the powder compact with a relative green density of 92.2%.

Compression temperature (K)	Strain rate (1/s)	RGD = 92.2%		
		Exp. PFS	Calc. PFS	Error (%)
623	0.01	34.5	34.4	0.2
623	0.1	44	46.3	5.3
623	1	58.5	58.2	0.5
623	10	69	70.1	1.6
673	0.01	21	20.7	1.6
673	0.1	31.5	32.6	3.3
673	1	43	44.4	3.4
673	10	57	56.3	1.2
723	0.01	13	8.8	32.3
723	0.1	20.5	20.7	0.9
723	1	30	32.6	8.6
723	10	45	44.5	1.2

peak flow stress of powder compacts with different relative green densities.

The ability of the model to predict the peak flow stress of powder compacts with different relative green densities was further evalu-ated by calculating the peak flow stress of a powder compact with a relative green density of 92.2% and comparing the calculated values to the experimental results (Table 6). The peak flow stresses of this powder compact were not used to develop the model. As shown in the table, the proposed model was able to predict accurately the peak flow stress of the powder compact. The average error and RMSE of the powder compact was 5% and 1.7 MPa, respectively.

4. Conclusions

(1) For the majority of compacts, the true stress-true strain curves obtained during the hot compression of Alumix 431D powder compacts with different relative green densities were characterised by a peak stress at a critical strain after which the flow stress remained nearly constant. This deformation behaviour can be attributed to the simultaneous occurrence of hardening mechanisms, such as strain and densification hardening, and softening mechanisms, such as dynamic recovery and recrystallisation, during deformation. As the strain rate and relative green density decreased or the deformation temperature increased, a decrease in the peak stress level was observed.

(2) The relationship between strain rate, deformation temperature, and the peak flow stress of a powder compact can be represented by the Zener–Hollomon parameter in an exponential equation containing relative green density compensated deformation activation energy (Q) and material constants (β and A). Depending on the relative green density, the deformation activation energy of the compacts ranged from 157 to 192 kJ/mol, which is in good agreement with the values reported for 7xxx series aluminium alloys.

(3) The relative green density has a significant influence on the hot deformation activation energy and β constant of a powder compact. As the relative green density increases, larger hot deformation activation energies and lower β constants were observed. The results of the present study showed that the presence of pores in the structures of porous materials reduces their resistance to deformation. In addition, the flow stress of powder compacts with high β constants is less sensitive to deformation parameters, such as deformation temperature and strain rate.

(4) The predicted and measured peak flow stresses of powder compacts were in good agreement, which confirms the applicability of the proposed equations for the prediction of hot deformation flow stresses of powder compacts with different relative green densities.

Acknowledgments

The authors would like to thank the Comunidad de Madrid for their financial support of this work through the ESTRUMAT Grant #S2009/MAT-1585.

References

[1] K. Lee, H. Kwon, Metall. Mater. Trans. A 33 (2002) 455–465.
[2] L.E.G. Cambronero, E. Sánchez, J.M. Ruiz-Roman, J.M. Ruiz-Prieto, J. Mater. Process. Technol. 143–144 (2003) 378–383.
[3] N. Jin, H. Zhang, Y. Han, W. Wu, J. Chen, Mater. Charact. 60 (2009) 530–536.
[4] I.A. MacAskill, A.D.P. LaDepha, J.H. Milligan, J.J. Fulton, D.P. Bishop, Powder Metall. 52 (2009) 304–310.
[5] W. Yuan, J. Zhang, C. Zhang, Z. Chen, J. Mater. Process. Technol. 209 (2009) 3251–3255.
[6] Y. Deng, Z. Yin, J. Huang, Mater. Sci. Eng. A 528 (2011) 1780–1786.
[7] R.E.D. Mann, R.L. Hexemer Jr., I.W. Donaldson, D.P. Bishop, Mater. Sci. Eng. A 528 (2011) 5476–5483.
[8] B. Verlinden, L. Froyen, TALAT Lecture 1401: Aluminium Powder Metallurgy, European Aluminium Association, Brussels, Belgium, 1994.
[9] G. O'Donnell, L. Looney, Mater. Sci. Eng. A 303 (2001) 292–301.
[10] C. Zubizarreta, S. Giménez, J.M. Martín, I. Iturriza, J. Alloys Compd. 467 (2009) 191–201.
[11] S. Serajzadeh, A. Karimi Taheri, Mech. Res. Commun. 30 (2003) 87–93.
[12] H. Mirzadeh, A. Najafizadeh, Mater. Sci. Eng. A 527 (2010) 1160–1164.
[13] G. Chunlei, X. Yongdong, W. Mengjun, Mater. Sci. Eng. A 528 (2011) 4199–4203.
[14] H. Zhang, L. Li, D. Yuan, D. Peng, Mater. Charact. 58 (2007) 168–173.
[15] X. Huang, H. Zhang, Y. Han, W. Wu, J. Chen, Mater. Sci. Eng. A 527 (2010) 485–490.
[16] M. Rajamuthamilselvan, S. Ramanathan, J. Alloys Compd. 509 (2011) 948–952.
[17] M.R. Rokni, A. Zarei-Hanzaki, A.A. Roostaei, A. Abolhasani, Mater. Des. 32 (2011) 4955–4960.
[18] W. Li, H. Li, Z. Wang, Z. Zheng, Mater. Sci. Eng. A 528 (2011) 4098–4103.
[19] G.Y. Lin, Z.F. Zhang, H. Zhang, D.S. Peng, J. Zhou, Acta Metall. Sinica (English Letters) 21 (2008) 109–115.
[20] H. Li, Z. Li, M. Song, X. Liang, F. Guo, Mater. Des. 31 (2010) 2171–2176.
[21] H.E. Hu, L. Zhen, L. Yang, W.Z. Shao, B.Y. Zhang, Mater. Sci. Eng. A 488 (2008) 64–71.
[22] M. yan Zhan, Z. Chen, H. Zhang, W. Xia, Mech. Res. Commun. 33 (2006) 508–514.
[23] P.T. Wang, M.E. Karabin, Powder Technol. 78 (1994) 67–76.
[24] P.T. Wang, Powder Technol. 66 (1991) 21–32.
[25] P.T. Wang, M.A. Zaidi, Powder Technol. 66 (1991) 9–19.
[26] L. Li, J. Zhou, J. Duszczyk, J. Mater. Process. Technol. 172 (2006) 372–380.
[27] C. Zener, J.H. Hollomon, J. Appl. Phys. 15 (1944) 22–32.
[28] E. Cerri, E. Evangelista, A. Forcellese, H.J. McQueen, Mater. Sci. Eng. A 197 (1995) 181–198.
[29] S. Liu, J. You, X. Zhang, Y. Deng, Y. Yuan, Mater. Sci. Eng. A 527 (2010) 1200–1205.